Cellular & Molecular Immunology (2017) 14, 223–234

www.nature.com/cmi

RESEARCH ARTICLE

Anti-tumor immunity of BAM-SiPc-mediated vascular photodynamic therapy in a BALB/c mouse model

Hing-Yuen Yeung[1], Pui-Chi Lo[2], Dennis K.P. Ng[3] and Wing-Ping Fong[1]

In recent decades, accumulating evidence from both animal and clinical studies has suggested that a sufficiently activated immune system may strongly augment various types of cancer treatment, including photodynamic therapy (PDT). Through the generation of reactive oxygen species, PDT eradicates tumors by triggering localized tumor damage and inducing anti-tumor immunity. As the major component of anti-tumor immunity, the involvement of a cell-mediated immune response in PDT has been well investigated in the past decade, whereas the role of humoral immunity has remained relatively unexplored. In the present investigation, using the photosensitizer BAM-SiPc and the CT26 tumor-bearing BALB/c mouse model, it was demonstrated that both cell-mediated and humoral adaptive immune components could be involved in PDT. With a vascular PDT (VPDT) regimen, BAM-SiPc could eradicate the tumors of ~70% of tumor-bearing mice and trigger an anti-tumor immune response that could last for more than 1 year. An elevation of Th2 cytokines was detected *ex vivo* after VPDT, indicating the potential involvement of a humoral response. An analysis of serum from the VPDT-cured mice also revealed elevated levels of tumor-specific antibodies. Moreover, this serum could effectively hinder tumor growth and protect the mice against further re-challenge in a T-cell-dependent manner. Taken together, these results show that the humoral components induced after BAM-SiPc-VPDT could assist the development of anti-tumor immunity.
Cellular & Molecular Immunology (2017) **14**, 223–234; doi:10.1038/cmi.2015.84; published online 21 September 2015

Keywords: anti-tumor immunity; damage-associated molecular patterns; humoral immunity; photodynamic therapy; tumor-bearing mice

INTRODUCTION

In cancer treatment, the successful induction of anti-tumor immunity has been shown to augment various therapies, including chemotherapy, cryotherapy, and radiotherapy.[1–3] Whether a cytotoxic treatment can trigger an anti-tumor immune response in the host in its course to eradicate the tumor is largely influenced by the treatment's ability to induce the expression of damage-associated molecular patterns (DAMPs) in tumor cells. DAMPs are molecules originally hidden inside the cell. They become exposed or released when the cell encounters certain stimuli, such as oxidative stress. Calreticulin (CRT), heat shock protein (HSP) 70, and HSP90 are well-known examples of DAMPs.[4] DAMP signals enable dying tumor cells to trigger the activation and maturation of dendritic cells (DCs). These activated DCs cross-present tumor-derived antigens to activate both $CD4^+$ T helper cells and $CD8^+$ cytotoxic T cells, which are responsible for killing tumor cells and establishing an immunological memory against the tumor.[4–6] The stimulatory role of DAMPs in the immune system was originally revealed in a chemotherapy study. Subsequently, DAMP signals were also found to be induced by other cytotoxic treatments, including high hydrostatic pressure, hyperthermia, and photodynamic therapy (PDT).[7–9]

PDT is a clinically approved treatment for various types of cancer.[6] In the process of PDT, patients are injected with a non-toxic photosensitizer (PS) that can be activated using light of a suitable wavelength. Upon photoactivation, the PS generates reactive oxygen species (ROS), such as singlet oxygen. Owing to their super-reactive nature, the effective range of ROS is less than 0.02 μm.[10] Inside the tumor, the primary cellular target of PDT is thus dependent on the localization of the PS during photoactivation. In classical PDT, the PS is allowed to diffuse freely and accumulate in the tumor. The primary target of such a treatment protocol is presumably the tumor cells.[11]

[1]School of Life Sciences, The Chinese University of Hong Kong, Shatin, N.T., Hong Kong, China; [2]Department of Biomedical Sciences, City University of Hong Kong, Tat Chee Avenue, Kowloon, Hong Kong, China and [3]Department of Chemistry, The Chinese University of Hong Kong, Shatin, N.T., Hong Kong, China
Correspondence: WP Fong, School of Life Sciences, The Chinese University of Hong Kong, Shatin, N.T., Hong Kong, China.
E-mail: wpfong@cuhk.edu.hk
Received: 24 February 2015; Revised: 15 July 2015; Accepted: 10 August 2015

In contrast, vascular PDT (VPDT) aims to disrupt the tumor-innervating vasculature by activating the PS while it is present in the vessel lumen. The PS could be targeted to the vessels by conjugation with specific peptides. Alternatively, blood vessel destruction could be achieved by activating the PS shortly after intravenous injection.[12–15]

Although the primary target of classical PDT is thought to be tumor cells, its action has also been shown to damage endothelial cells and possibly tumor-residential immune cells, such as tumor-associated macrophages.[13,16–21] As a result, PDT could lower the tumor load and, at the same time, assist the development of anti-tumor immunity by cellular factors released from the disrupted tumor stroma (for example, DAMPs) and the removal of pro-tumoral immune cells.[5,22–24] In the initial study showing that the classical PDT-induced immune response could protect the host from post-treatment cancer relapse, T cells were found to be indispensable.[25,26] However, the role of another component of the adaptive immune system, B cells, remains poorly addressed in the context of PDT.[24]

In VPDT, the primary target of the treatment is shifted from the tumor cells themselves to their associated endothelium. The activation of a PS inside the vessel lumen could induce an instant occlusion of blood flow, which correlates with the therapeutic outcome of VPDT.[14,26,27] Nevertheless, VPDT does not damage endothelial cells alone. Extensive tumor necrosis usually results after this treatment procedure.[28,29] In one study, VPDT could even remove the existing tumor-residential T-cell population.[13] However, it remains unclear whether the tumor cell death associated with VPDT is secondary to the obstructed blood supply or is directly caused by leakage of the PS from the ruptured endothelium during the photosensitization period.[21] Similar to classical PDT, VPDT has also been reported to stimulate anti-tumor immunity.[13,30] Depending on the tumor model and PS used, an additional immunomodulatory agent, such as cyclophosphamide, might be required to induce optimal VPDT-mediated anti-tumor immunity.[31] At present, the difference between classical PDT and VPDT in terms of their immunomodulatory effect, if there is any, remains largely elusive.[31]

The treatment protocol affects the therapeutic effect of a PS. For instance, hypericin and hexamethylhypericin have higher curative rates in VPDT, whereas Photofrin, tetrabromohypericin, and Foslip work better in classical PDT.[32–35] In the past decade, we have synthesized a number of novel PSs. Among them, BAM-SiPc, an unsymmetrical bisamino silicon(IV) phthalocyanine, is one of the most potent PSs.[36] BAM-SiPc was non-toxic in the dark at concentrations as high as 4 mM; however, with illumination, it showed an IC_{50} value of ~20 nM toward various cell lines.[36–38] The photo-cytotoxic effect of BAM-SiPc has also been studied in the tumor-bearing nude mouse model using a classical PDT protocol. The results showed that BAM-SiPc could significantly reduce the size of HepG2 tumors and retard the growth of HT29 tumors with no apparent hepatic or cardiac injury.[39] Unfortunately, BAM-SiPc did not show any specificity toward the tumor tissue. Nevertheless, its potent photodynamic activity, apparent lack of dark toxicity/side effects and short retention time render BAM-SiPc a promising candidate for further study.[39]

In the present investigation, the clinical potential of BAM-SiPc as a VPDT agent was evaluated. BALB/c mice bearing the syngeneic mouse colon tumor CT26 were employed. The abilities of BAM-SiPc to trigger vascular destruction, tumor ablation, and anti-tumor immunity in terms of both cellular and humoral immune responses were examined.

MATERIALS AND METHODS

Preparation of BAM-SiPc

BAM-SiPc was synthesized according to the procedure of Lo *et al*.[36] For *in vitro* assays, a BAM-SiPc stock solution was prepared by dissolving BAM-SiPc powder in dimethylformamide (494488, Sigma-Aldrich, St. Louis, MO, US), followed by a 10-fold dilution using 0.01 M aqueous Cremophor EL (C5135, Sigma-Aldrich, St. Louis, MO, US). The stock solution was further diluted to suitable concentrations using complete RPMI-1640 medium (23400021, Invitrogen, Carlsbad, CA, US). For *in vivo* assays, BAM-SiPc powder was dissolved in DCP solvent (dimethylformamide/0.01 M aqueous Cremophor EL/phosphate-buffered saline (PBS); 1:9:10, v/v/v) before being used.

Cell line and culture conditions

CT26 murine colon tumor cells were obtained from the American Type Culture Collection (CRL-2638, ATCC, Manassas, VA, US). The cells were maintained in RPMI-1640 medium supplemented with glucose (2.5 g L^{-1}, D9434, Sigma-Aldrich, St. Louis, MO, US), 10% fetal bovine serum (FBS, Invitrogen, 16000044), sodium pyruvate (1 mM, 11360070, Invitrogen, Carlsbad, CA, US) and a penicillin (100 U mL^{-1})/streptomycin (100 μg mL^{-1}) mix (15140122, Invitrogen, Carlsbad, CA, US). For cytokine profiling and the lymphocyte cytotoxicity assay, splenocytes were obtained from BALB/c mice and were maintained in the above medium except that (i) no glucose or pyruvate was added, and (ii) heat-inactivated FBS was used instead of normal FBS.

In vitro photodynamic treatment

CT26 cells (2×10^4 cells per well) were seeded onto a 96-well plate and were incubated overnight at 37 °C in a humidified 5% CO_2 incubator. The cells were incubated with BAM-SiPc in the dark for 2 h. After being washed with PBS and replenished with complete RPMI-1640 medium, the cells were illuminated with a halogen lamp (300 W) for 20 min at room temperature. Light with $\lambda < 610$ nm was cut off by a red glass filter (Newport, Irvine, CA, US). The fluence rate used was 100 mW/cm^2, giving a total fluence of 120 J/cm^2 for the process. A beaker of water was placed between the lamp and the sample to absorb the heat emitted from the lamp. No observable temperature change was detected in the sample after an illumination period of 20 min.

Cell proliferation assay

After *in vitro* PDT, the CT26 cells were incubated overnight at 37 °C in a humidified 5% CO_2 incubator. Subsequently, 3-(4,5-dimethylthiazol-2-yl)-2,5-diphenyltetrazolium bromide (MTT)

(50 μL, 3 mg mL^{-1} in PBS, 19265, USB, Cleveland, OH, US) was added to each well, followed by incubation for 90 min at 37 °C. Sodium dodecyl sulfate (50 μL, 10% w/v, 75819, USB, Cleveland, OH, US) was added, followed by further incubation for 30 min. Afterwards, the contents of each well were mixed with 80 μL of isopropanol. The absorbance at 540 nm was measured using a plate reader (SpectraMax).

DAMP detection (confocal microscopy)

CT26 cells (4×10^4) were seeded in a 35 mm culture dish with a glass bottom (0.085–0.13 mm in thickness) designed for confocal microscopic applications (P35G-0-14-C, MatTek, Ashland, MA, US). Four hours after various treatments, the cells were washed twice with PBS and were stained with anti-CRT (ab2907, Abcam, Milton, Cambridge, UK), anti-HSP70 (ab31010, Abcam, Milton, Cambridge, UK), or anti-HSP90 (ab13495, Abcam, Milton, Cambridge, UK) antibodies for 1 h at 4 °C. The staining solution was prepared by diluting the respective antibodies in staining buffer (10% heat-inactivated FBS in PBS) (1:100, v/v). Samples were washed twice with PBS before being fixed with cold methanol for 10 min at –20 °C. After two PBS washes, the cells were stained with an Alexa-488-conjugated secondary antibody (1:100, v/v, A11034, Invitrogen, Carlsbad, CA, US) together with an anti-cadherin antibody (sc-59876, Santa Cruz Biotechnology, Santa Cruz, CA, US) overnight at 4 °C. After two PBS washes, the cells were stained with an Alexa-633-conjugated secondary antibody (1:100, v/v, A21052, Invitrogen, Carlsbad, CA, US) and Hoechst 33342 (10 mg mL^{-1}, B2261, Sigma-Aldrich, St. Louis, MO, US) (1:10,000, v/v) overnight at 4 °C. The samples were rinsed with PBS twice before being examined under a confocal microscope (Olympus FV1000 IX81-TIRF).

DAMP detection (flow cytometry)

PDT was performed on 1×10^6 CT26 cells in a 60 mm culture dish. Cells were collected by trypsinization 4 h later and were stained with the DAMP-specific primary antibodies (1:1000, v/v) as described above, together with propidium iodide (1:500, v/v, 2 mg mL^{-1}, 81845, Sigma-Aldrich, St. Louis, MO, US) in 0.5 mL of staining buffer for 1 h at 4 °C. After being washed with PBS, the cells were stained with an Alexa-488-conjugated secondary antibody (1:500, v/v) in 0.1 mL of staining buffer for 30 min at 4 °C. After another wash with PBS, the samples were subjected to flow cytometric analysis (FACSVerse, BD Biosciences).

BALB/c mouse model

Female BALB/c and nude mice, 8–10 weeks of age, were obtained from the Laboratory Animal Services Centre at The Chinese University of Hong Kong. To establish the tumor-bearing mouse model, 1×10^6 CT26 tumor cells were subcutaneously injected into the backs of the mice. The BALB/c mice were shaved in the tumor region using a razor blade 11 days after tumor inoculation. The tumor size was monitored by measuring the length and width of the tumor using a Vernier caliper (tumor size = length × $width^2/2$). When the tumor grew to a length greater than 12 mm, the mouse was euthanized by cervical dislocation. All the procedures were approved by the University Animal Experimentation Ethics Committee.

Histological analysis

BAM-SiPc solution (1.3 mg kg^{-1}, 200 μL per mouse) was injected into the tail veins of the CT26 tumor-bearing BALB/c mice 20 min or 24 h before the mice were sacrificed. To visualize the blood vessel, a FITC-conjugated anti-CD31 antibody (RM5201, Invitrogen, Carlsbad, CA, US) was also intravenously injected into the mice 4 h before the mice were killed. The tumors were excised and snap frozen in optimal cutting temperature compound (4583, TissueTek, St. Torrance, CA, US). Tumor sections 5 μm in thickness were viewed immediately under a confocal microscope. BAM-SiPc was visualized using an excitation laser at 633 nm and an emission filter at 665–680 nm.

The presence of specific markers in the tumor was analyzed using a cryo-histological approach. At the indicated times after VPDT, the tumor was excised and snap frozen in optimal cutting temperature compound. Tumor sections 5 μm in thickness were fixed with 4% paraformaldehyde (P6148, Sigma-Aldrich, St. Louis, MO, US) for 15 min at room temperature. After being washed twice with PBS, the samples were stained with primary antibody together with Hoechst 33342 (1:1000, v/v) for 2 h at room temperature. After two washes with PBS, the samples were stained with secondary antibody for 1 h at room temperature. Following two more washes with PBS, the samples were viewed under a confocal microscope. The primary antibodies used include those against CRT (1:100, v/v), CD31 (1:150, v/v, ab28364, Abcam, Milton, Cambridge, UK), CD11c (1:100, v/v, 553801, BD Biosciences, San Jose, CA, US) and a CD4/CD8 mix (1:100, v/v, 558391, BD Biosciences, San Jose, CA, US), and all were diluted with the staining buffer.

Alternatively, the tumors excised from the mice were fixed in 4% paraformaldehyde overnight at 4 °C. After being dehydrated in 70% ethanol for 1 day, the tumors were embedded in paraffin and sections 8 μm in thickness were prepared. The de-paraffinized sections were subjected to heat-mediated antigen retrieval in 10 mM sodium citrate solution (pH 6.0) at 95 °C for 10 min and were then allowed to equilibrate to room temperature. The samples were treated with 3% H_2O_2 for 8 min and blocked with 10% heat-inactivated FBS for 1 h at room temperature. After overnight staining with primary antibody at 4 °C and then with horseradish peroxidase-conjugated secondary antibody for 1 h at room temperature, the color was developed by incubation with 3,3′-diaminobenzidine (K346811, Dako, Carpinteria, CA, US), followed by counterstaining with hematoxylin. The primary antibodies used include those against CRT and B220 (48-0452-82, eBioscience, San Diego, CA, US). Images were captured using a cooled digital color camera (Olympus DP72).

***In vivo* photodynamic treatment**

BAM-SiPc was injected intravenously through the tail vein into the BALB/c mice (1.3 mg kg^{-1}, 200 μL per mouse). After 20 min, a PDT laser beam (Ceralas PDT 675 medical laser system, CeramOptec GmbH, Biolitec group, Germany) was spotted directly onto the tumor region at a fluence rate of

0.1 W/cm^2 for 10 min, giving a total fluence of 60 J/cm^2. The tumor sizes of the mice were monitored for the next 21 days. VPDT group, $n = 28$; control group, $n = 18$.

Tumor re-challenge test

On Day 21 after VPDT, CT26 cells (1×10^6) were injected subcutaneously into the other side on the back of the BALB/c mice in both the cured ($n = 19$) and relapsed ($n = 8$) groups. The size of the second tumor was monitored for 12 days. The same batch of CT26 cells was also injected into naïve mice (i.e., mice without the first tumor) to ensure the tumorigenicity of the tumor cells, $n = 6$. The cured mice were re-challenged again on Day 120 or Day 400 after VPDT, $n = 4$. A naïve mice control was included in each experiment, $n = 4$.

Cytokine profiling

On Day 30 after the tumor re-challenge, four mice that had remained tumor-free were sacrificed by cervical dislocation. Splenocytes were obtained by squeezing the spleen through a 40 μm nylon cell strainer and were washed with PBS. Red blood cells were lysed by incubation with ACK buffer (154 mM NH_4Cl, 10 mM $KHCO_3$, and 0.1 mM EDTA, pH 7.4) at 4 °C for 10 min and were then removed by being washed with PBS. Splenocytes (2.5×10^6 cells per well) were seeded into a 96-well plate together with CT26 cells (5×10^4 cells per well) for a 24-h co-culture. Afterwards, supernatants were obtained and stored at –80 °C for further analysis of various cytokines, including (i) interferon gamma (IFN-γ), (ii) tumor necrosis factor alpha (TNF-α), (iii) interleukin (IL)-4, and (iv) IL-10, using the corresponding ELISA kits (EM007-96, ExCell, Shanghai, China, EM008-96, ExCell, Shanghai, China, KA0252, Abnova, Heidelberg, Germany, and EM005-96, ExCell, Shanghai, China, respectively).

Lymphocyte cytotoxicity assay

Splenocytes were obtained from the tumor-free mice 40 days after the tumor re-challenge test and were used as the effector in a lymphocyte cytotoxicity assay with a carboxyfluorescein diacetate succinimidyl ester (CFSE, C34554, Invitrogen, Carlsbad, CA, US)-based protocol. Briefly, CT26 cells were separated into two portions, viz. target and reference. CT26 cells (1×10^6) were stained with 0.1 μM (target) or 1 μM (reference) of CFSE in PBS supplemented with 1% heat-inactivated FBS for 3 min at room temperature, followed by a wash with 1 mL of culture medium. Target and reference cells (1×10^5) were plated separately into a 96-well plate. Splenocytes were added to the target cells at effector-to-target ratios of 0:1 and 50:1 and were incubated for 4 h at 37 °C. The target-splenocyte mix and reference cells were mixed and subjected to flow cytometric analysis.

Target ($FITC_{dim}$) and reference ($FITC_{bright}$) cells were gated. The cytotoxicity of the splenocytes was estimated using the following formula: % cytotoxicity = [1– (T'/R') × (R/T)] × 100%, where T and R are the amount of the target ($FITC_{dim}$) and reference ($FITC_{bright}$) populations, respectively, when the splenocyte-to-tumor cell ratio is 0:1, and T' and R' are the corresponding values when the ratio is 50:1.

Serum extraction

To boost the production of anti-CT26 antibody, CT26 cells (1×10^6) were injected subcutaneously into the VPDT-cured mice on Day 180 after VPDT. Boosting was not performed for the control mice because they either bore tumors already or served only as the naïve control. The mice were sacrificed 7 days later, and blood was obtained by cardiac puncture. The serum prepared from the clotted blood was stored at –80 °C until further analysis.

Detection of anti-CT26 antibodies

Mouse serum was diluted to 3% with staining buffer containing propidium iodide (1:500, v/v). CT26 cells (1×10^5) were added and incubated at 4 °C for 1 h with occasional shaking. After being washed with PBS, the tumor cells were resuspended in Alexa-488-conjugated anti-mouse antibody (A11029, Invitrogen, Carlsbad, CA, US) diluted in staining buffer (1:500, v/v). After being incubated at 4 °C for 30 min, the cells were washed with PBS and subjected to flow cytometric analysis.

Anti-tumor effect of anti-CT26 antibody and the presence of anti-tumor immunity

Mouse serum samples were diluted 1:4 with PBS and were filtered through a 0.22 μm filter (4602, Pall, Port Washington, NY, US). The filtrate was mixed with 2×10^5 CT26 cells and injected subcutaneously into the flank of the BALB/c mice, $n = 5$, 14, and 6 for mice receiving sera from naïve, VPDT-cured, and VPDT-relapsed mice, respectively. PBS was used instead of serum as the control, $n = 11$. Tumor growth was monitored for 20 days.

On Day 20, the mice that had been treated with serum from VPDT-cured mice were re-challenged with 1×10^6 CT26 cells at a second site, $n = 11$. Naïve mice controls were included to ensure the tumorigenicity of the tumor cells, $n = 4$. The size of the second tumor was monitored for 12 days. Afterwards, mice that had successfully resisted the tumor re-challenge were subjected to the T-cell dependency test (see below), $n = 3$.

The effect of serum from the VPDT-cured mice on the establishment of CT26 tumors was also tested in nude mice, $n = 5$ for both the experimental group and the naïve mice control group. On Day 20, the mice in the experimental group were re-challenged with 1×10^6 CT26 cells at a second site, and the tumor size was monitored for 12 days, $n = 4$.

T-cell dependency test

BALB/c mice that had resisted tumor growth in the re-challenge test, after either VPDT or serum treatment, were given an intraperitoneal injection of 3 μg of anti-CD3 antibody (16003285, eBioscience, San Diego, CA, US) on Days –1, 0, 2, and 4. On Day 0, 1×10^6 CT26 cells were subcutaneously inoculated into the mice, and the tumor size was monitored for 12 days.

Statistical analysis

The data were analyzed using a *t*-test performed with SigmaPlot ver. 12.0. Results with *p* values < 0.05 were considered significant; $*p < 0.05$; $**p < 0.005$; ns, not significant.

RESULTS

BAM-SiPc-PDT could induce DAMP expression *in vitro*

The photodynamic activity of BAM-SiPc was tested using the murine CT26 cell line. A dose-dependent cytotoxic effect was observed upon illumination, with an IC_{50} value of less than 10 nM; this effect was not observed in the dark (Figure 1a). Subsequently, the DAMP expression profile was analyzed using confocal microscopy. CRT, HSP70, and HSP90 were detected on the tumor cell surface 4 h after PDT treatment (Figure 1b). A flow cytometric analysis was performed to quantify the numbers of cells expressing different DAMPs. After PDT, the population of cells expressing surface CRT, HSP70, and HSP90 was increased by more than 3-fold (Figure 1c).

VPDT could destroy tumor vasculature and induce DC infiltration into CT26 tumors

The intra-tumoral bio-distribution of BAM-SiPc in the CT26 tumor-bearing mice was studied. A histological analysis of the cryo-sections showed a good co-localization of PS with the blood vessel 20-min post-injection. In contrast, a more dispersed localization of PS was observed 24-h post-injection (Figure 2a). VPDT was performed with a short drug–light interval (the time lag between drug and light application) of 20 min. The effect of this VPDT procedure on the tumor blood vessel was examined under a confocal microscope. The tumor-associated endothelium ($CD31^+$) became barely visible 16 h after treatment (Figure 2b). At the same time, the CRT level of the tumor was up-regulated and tumor-infiltrating DCs ($CD11c^+$ cells) were detected (Figure 2c). The CRT signal could be detected on the tumor cell surface as early as 30 min after treatment. This signal could still be observed 24 h later (Figure 2d).

VPDT led to tumor regression and the development of anti-tumor immunity

The anti-tumor effect of BAM-SiPc-VPDT was investigated by monitoring the sizes of the tumors in CT26 tumor-bearing BALB/c mice. The tumor size was 222 ± 100 mm^3 before the treatment. For all 28 mice in the VPDT group, the tumors regressed quickly and disappeared completely within 5 days. Among these mice, 20, representing ~70% of the VPDT group, remained tumor free throughout the entire observation period up to Day 21 post-VPDT (Figure 3a). Tumor relapse was observed in 8 mice. Nevertheless, the tumors grew more slowly, such that in the VPDT-relapse group, the tumor size reached

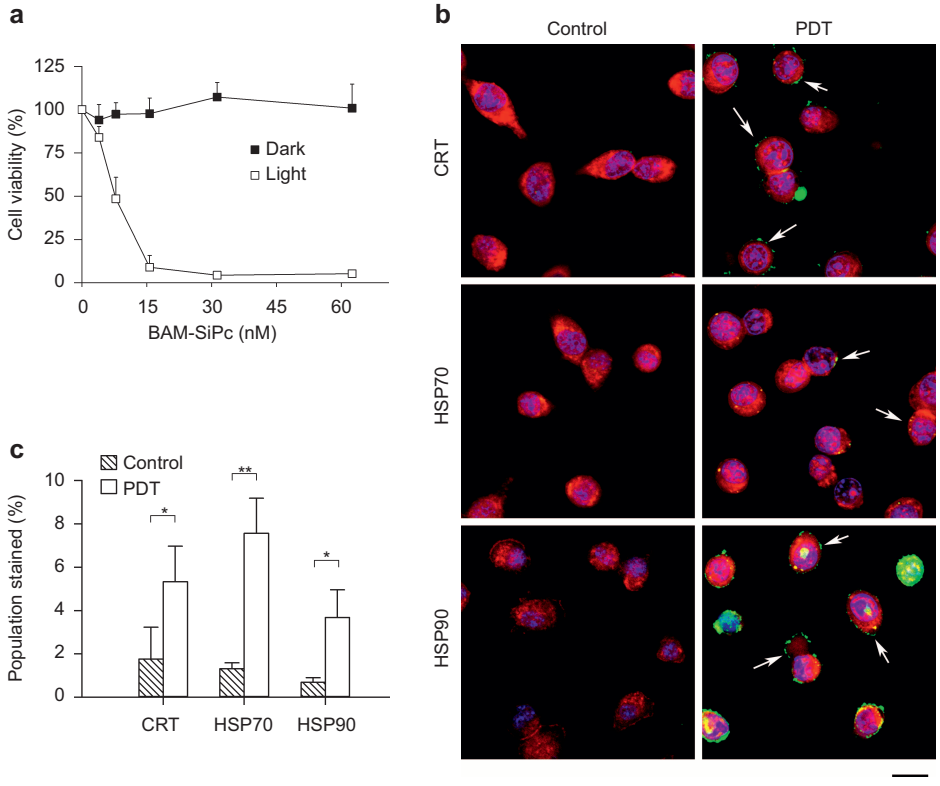

Figure 1 DAMP induction of BAM-SiPc-PDT *in vitro*. (**a**) Cytotoxicity. Different concentrations of BAM-SiPc were incubated with CT26 cells. The cytotoxic effects of BAM-SiPc against the CT26 cells with or without light illumination are shown as the means with S.E.M. of three independent experiments. (**b**) DAMP expression (confocal microscopy). PDT was performed with 10 nM BAM-SiPc, and the cells were allowed to stand for 4 h. CT26 cells were stained with Hoechst 33342 (blue), an antibody against cadherin (red) and antibodies against CRT, HSP70, or HSP90 (green). Arrows indicate the locations of DAMPs. Bar = 10 μm. (**c**) DAMP expression (flow cytometry). At 4-h post-PDT, cells were stained with propidium iodide and antibodies against various DAMPs. The population undergoing immunogenic cell death (propidium $iodide^{-ve}$/$DAMPs^{+ve}$) is shown as the mean with S.D. of three independent experiments. *$p < 0.05$; **$p < 0.005$.

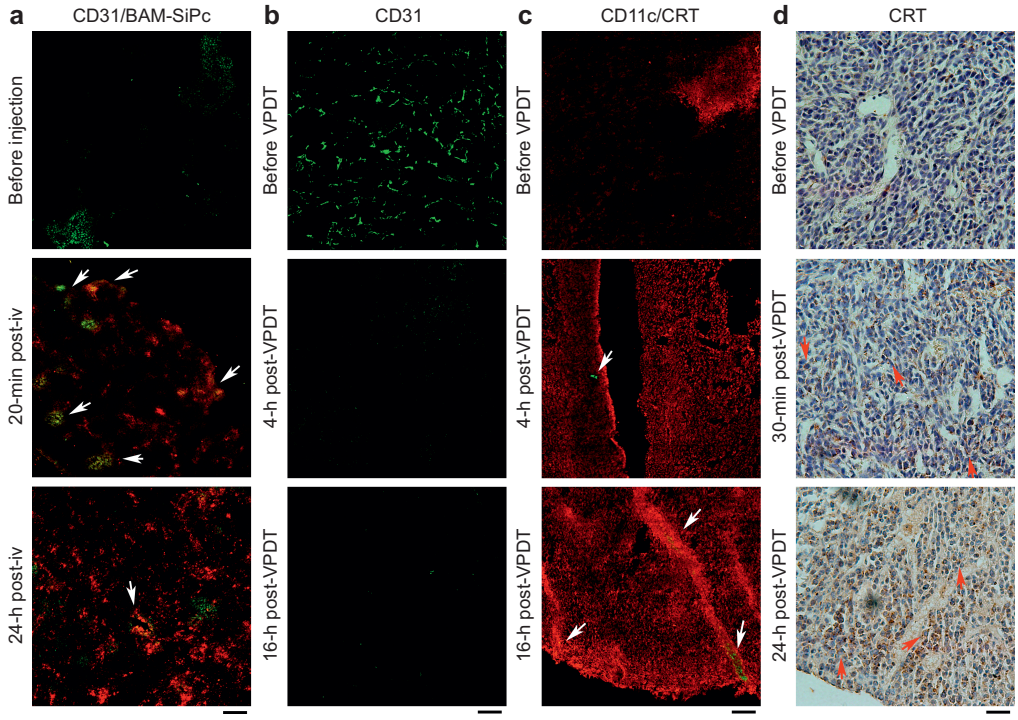

Figure 2 Tumor vasculature destruction and DAMP induction after VPDT. (**a**) Intra-tumoral bio-distribution of BAM-SiPc. A FITC-conjugated anti-CD31 antibody and BAM-SiPc were intravenously injected into the mice. At the indicated times, 5 μm cryo-sections of CT26 tumors were viewed under a confocal microscope. Arrows indicate regions of overlap between the BAM-SiPc and blood vessel signals. (**b**) Blood vessel destruction. At the indicated times post-VPDT, CT26 tumor sections were stained with an anti-CD31 antibody (green). (**c**) CRT expression and DC infiltration. Tumor sections were stained with antibodies against CRT (red) and CD11c (green). Arrows indicate the locations of DCs. (**d**) CRT expression on the tumor cell surface. Paraffin tumor sections were stained with an antibody against CRT (brown). Arrows indicate cells expressing CRT on the surface. Bar = 120 μm (**a**, **b**, and **c**) or 100 μm (**d**).

the experiment end point, i.e., a tumor length >12 mm, at a much later time (28.4 ± 9.2 days) than in the control group (11.5 ± 5.3 days) (Figure 3b). It remains unclear why some mice suffered from tumor relapse; the initial tumor size appears not to be the reason. The initial tumor size was actually slightly larger in the VPDT-cured mice (237 ± 113 mm^3) than in the mice showing relapse (186 ± 54 mm^3), although this difference was not statistically significant ($p > 0.4$) (data not shown).

The presence of anti-tumor immunity was tested in the VPDT-treated mice in a re-challenge experiment. All the VPDT-cured mice, except one, resisted re-challenge and remained tumor free for up to 400-day post-VPDT (data not shown). In contrast, all the mice in the VPDT-relapse group developed a second tumor. Nevertheless, the second tumor grew much more slowly than in the naïve controls. On Day 12 after the second inoculation, i.e., Day 33 post-VPDT, the size of the second tumor in the VPDT-relapse group was 49 ± 43 mm^3, compared with 184 ± 46 mm^3 in the controls (Figure 3c). A longer-term growth curve of the second tumor could not be obtained because the size of the original tumor had already reached the end point of the experiment.

The long-term immunological memory against the tumor was tested by another round of re-challenge on Day 120 or Day 400 post-VPDT. All four of the mice that had resisted the first tumor re-challenge were able to reject the newly implanted tumors in these tests (data not shown).

VPDT resulted in elevation of both Th1 and Th2 cytokines

Cytokine profiles were evaluated *ex vivo* in a co-culture system composed of CT26 tumor cells and splenocytes obtained from VPDT-cured mice. The cytokines examined included those responsible for stimulating the Th1 (IFN-γ and TNF-α) and Th2 (IL-4 and IL-10) immune responses. The results showed that all four cytokines were elevated by more than 6-fold in the VPDT-cured group compared to the controls (Figure 4).

T cells were essential to the VPDT-triggered anti-tumor immunity

The involvement of T cells was studied histologically by examining tumor sections obtained after VPDT. $CD4^+$ T cells were found at the tumor rim 4 h after VPDT, and $CD8^+$ T cells were also observed 16 h after VPDT (Figure 5a). In addition, splenocytes were isolated from the VPDT-cured mice to evaluate their cytotoxic effect against CT26 tumor cells in a mixed lymphocyte reaction. The cytotoxicity of splenocytes against the CT26 cells in the VPDT-cured mice was ~3 times more potent than that in the controls (Figure 5b). The importance of T cells in the anti-tumor immunity was examined using the T-cell depletion test. Re-challenge of the VPDT-cured mice with

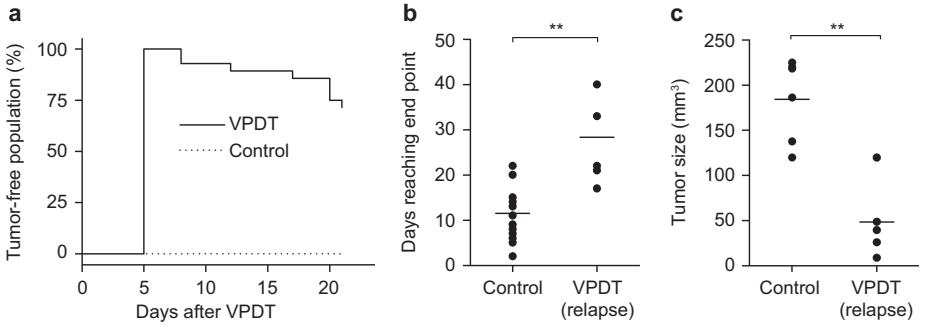

Figure 3 Therapeutic effects of BAM-SiPc-VPDT. (**a**) Cure rate. On Day 11 post-tumor inoculation, mice were treated with VPDT with a drug–light interval of 20 min. The tumor growth in the population was monitored up to Day 21. VPDT, $n = 28$; controls, $n = 18$. (**b**) Delayed tumor growth in the VPDT-relapse mice. The time for the relapsed tumor to reach the end point of the experiment (tumor length > 12 mm) was compared between the VPDT-relapse population ($n = 8$) and the controls ($n = 18$). (**c**) Post-VPDT anti-tumor immunity. On Day 21 post-VPDT, 1×10^6 CT26 tumor cells were inoculated into the mice in the opposite flank. The size of the second tumor on Day 12 after re-challenge was compared between the VPDT-relapse group ($n = 5$) and the naïve control group ($n = 6$). The line represents the mean value in the vertical scatter plot. $^{**}p < 0.005$.

CT26 tumor cells resulted in tumor growth when T cells were depleted with an antibody specific to the pan-T-cell marker CD3 (Figure 5c).

Serum obtained from VPDT-cured mice assisted the development of T-cell-dependent anti-tumor immunity

The presence of tumor-infiltrating B cells after VPDT was examined using a histological approach by staining the mouse pan-B-cell marker B220. Infiltration of B cells was observed at the tumor rim 30 min after treatment (Figure 6a). A flow cytometric approach was also used to evaluate the presence of tumor-specific antibodies in the serum of the VPDT-treated mice. The population of CT26 cells stained by the serum of the VPDT-cured mice was increased by 3.5-fold compared with that stained by the serum of the naïve control mice; however, the increase was only marginal for the serum obtained from VPDT-relapse mice (Figure 6b). The tumor-suppressive effects of these sera were then evaluated *in vivo*. The sera were mixed with CT26 cells and injected into the mice, and subsequent tumor growth was monitored. Mice receiving serum from naïve mice or VPDT-relapse mice did not show any obvious difference in tumor growth compared with the PBS (i.e., serum-free) control. In contrast, serum obtained from the VPDT-cured mice could suppress the tumor growth. On Day 20 post-inoculation, the tumor size was ~50% of that in the controls. However, such serum failed to suppress tumor growth in nude mice (Figure 6c).

The immunomodulatory potential of serum from the VPDT-cured mice was examined. BALB/c mice receiving the serum of VPDT-cured mice were given the first re-challenge of CT26 tumor cells at a second site. These mice could resist the growth of the second tumor. On Day 12 post-inoculation of the second tumor, no tumor mass could be observed at this site. However, when their T cells were depleted with an anti-CD3 antibody, the mice could no longer resist tumor growth in the second re-challenge of CT26 tumor cells. In nude mice, the serum of VPDT-cured mice failed to induce anti-tumor immunity; a second tumor developed as the same rate as in the controls in the re-challenge test (Figure 6d). The immunomodulatory effects of sera on the tumor cells were examined. Treatment with the serum of VPDT-cured mice, but not naïve mice, resulted in the expression of surface CRT on CT26 cells *in vitro* (Figure 6e).

DISCUSSION

The CT26 tumor mouse model has been used to study the immunomodulatory effects of various anti-cancer treatments,

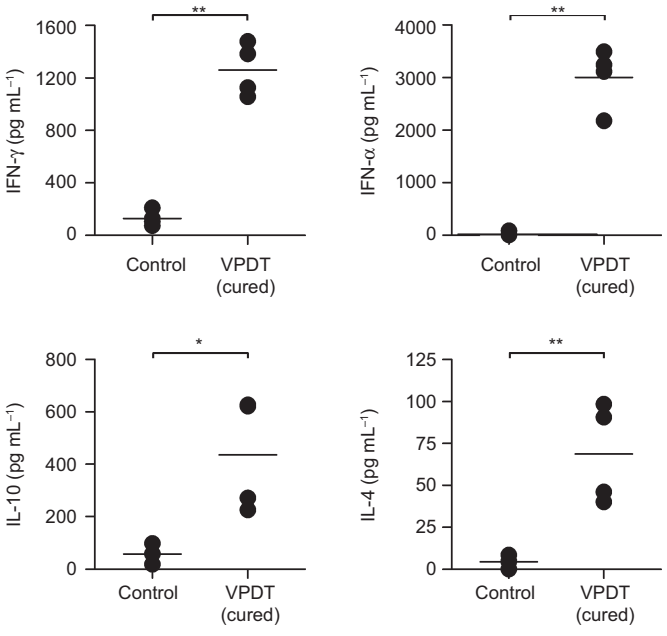

Figure 4 *Ex vivo* cytokine profile. VPDT-cured mice that had successfully resisted re-challenge of tumor cells were used. Splenocytes were obtained 30 days after the re-challenge test. After the red blood cells were removed, the splenocytes were mixed with CT26 cells and incubated for 24 h. The supernatant was collected for analyses of Th1 (IFN-γ, TNF-α) and Th2 (IL-4, IL-10) cytokines using ELISA kits. VPDT-cured mice and controls, $n = 4$. The line represents the mean value in the vertical scatter plot. $^{*}p < 0.05$; $^{**}p < 0.005$.

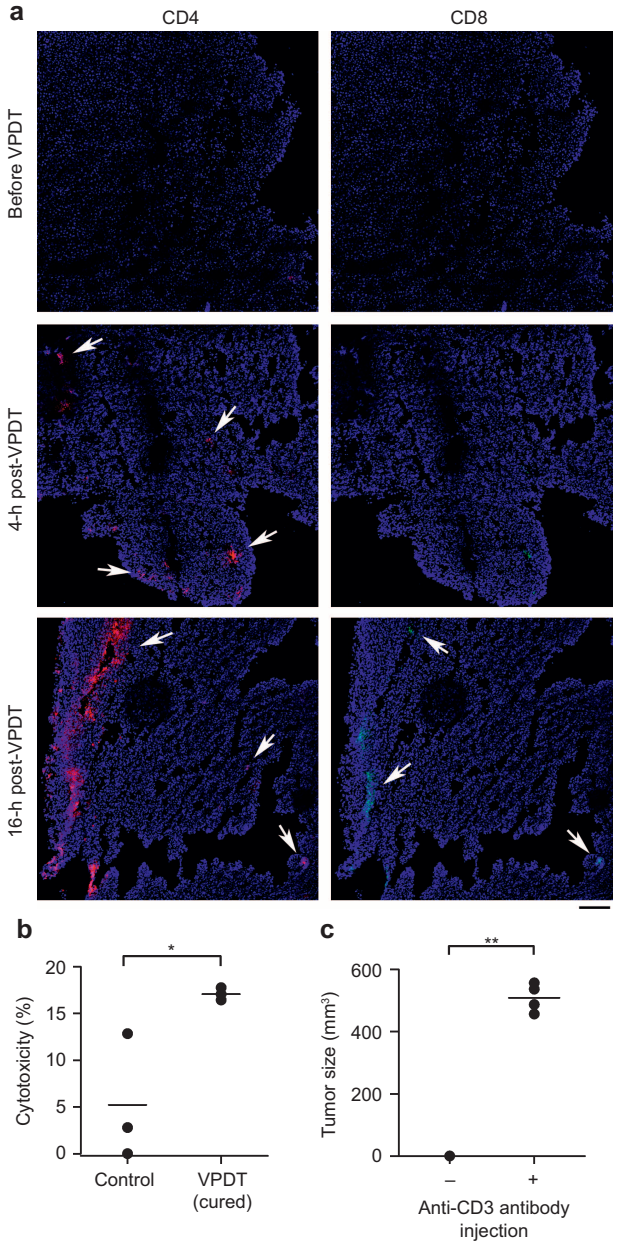

Figure 5 Involvement T cells in the VPDT-mediated immune response. (**a**) T-cell infiltration. Tumor sections obtained at different times after VPDT were stained with antibodies against CD4 (red), CD8 (green), and Hoechst 33342 (blue). Arrows indicate the sites of infiltration. Bar = 120 μm. (**b**) Splenocyte cytotoxicity. On Day 40 post-tumor re-challenge, the tumor-free mice were sacrificed. Their splenocytes were used as the effector with CT26 cells as the target. The two cell types were mixed at a ratio of 50:1 and incubated for 4 h. The cytotoxicity of the splenocytes was evaluated using flow cytometry, $n = 3$. (**c**) T-cell-dependent immunological memory. Mice that had been cured by VPDT and were resistant to tumor re-challenge ($n = 4$) were depleted of T cells by intraperitoneal injections of an anti-CD3 antibody. These mice were then re-challenged with 1×10^6 CT26 cells. The tumor sizes were recorded on Day 12 post-inoculation. The line represents the mean value in the vertical scatter plot. $*p < 0.05$; $**p < 0.005$.

including chemotherapy and radiotherapy.[1,7,40] This tumor is known to secrete transforming growth factor-β, which hampers the development of anti-tumor immunity by strengthening the action of regulatory T (Treg)-cell populations. As a result, this model is prone to tumor relapse after VPDT although the tumor itself expresses the tumor antigen gp70.[41]

It has been reported that verteporfin-VPDT could achieve tumor-free survival together with an induction of immunological memory (i.e., a complete response) in cell lines that bear a tumor rejection antigen, for example, RIF-1 tumors with EGFP in C3H/HeN mice, P815 tumors with P1A antigen in DBA/2 mice, or with the depletion of Treg cells in J774 tumors in BALB/c mice.[31,42,43] However, when CT26 tumors were treated with verteporfin, a complete response could be achieved only when repetitive low doses of cyclophosphamide were administered to deplete the Treg population.[41] Alternatively, an additional foreign antigen, such as β-galactosidase, must be transfected into the tumor cells to strengthen its immunogenicity before the treatment.[45]

In contrast, some other PSs (for example, hypericin and WST11[13,30]) could trigger a complete response in the CT26 tumor model without the aid of extra immunomodulatory agents. WST11-VPDT could deplete the tumor-associated T-cell population, which possibly includes Treg cells. Moreover, novel antigens could be induced on CT26 tumor cells after VPDT, as indicated by the presence of new protein bands in the post-PDT tumor cell lysate recognized by the mouse serum.[13] Taken together, these results indicate that the presence of relevant tumor antigens and the depletion of Treg cells could both be important for the induction of a complete response following VPDT.

In the present investigation, VPDT was performed using BAM-SiPc. To achieve VPDT, the PS is usually activated shortly after intravenous administration.[13,30,44,45] With a drug–light interval of 20 min, a good co-localization between BAM-SiPc and the tumor blood vessel was observed (Figure 2a). This treatment successfully destroyed the tumor vasculature (Figure 2b) and was similar to hypericin and WST11 in promoting tumor-free survival and triggering the development of anti-tumor immunity.[13,30]

The anti-tumor efficacy of BAM-SiPc was previously tested in HepG2 and HT29 tumor-bearing nude mice using the long drug–light interval (24 h) classical protocol. This treatment could only dampen the tumor growth but could not completely eradicate the tumors.[39] Thus, it appears that BAM-SiPc works better in VPDT than in classical PDT conditions. The higher tumor ablation rate in VPDT is not likely to be due to the presence or absence of a functional immune system in the mouse model, as better performance of VPDT compared with classical PDT for some PSs has been demonstrated in both immunodeficient and immunocompetent mice.[32–34,46] Although the mechanisms governing the preference of a particular PS toward a specific PDT protocol require further investigation, the present study demonstrated that a fairly good therapeutic outcome could be achieved by

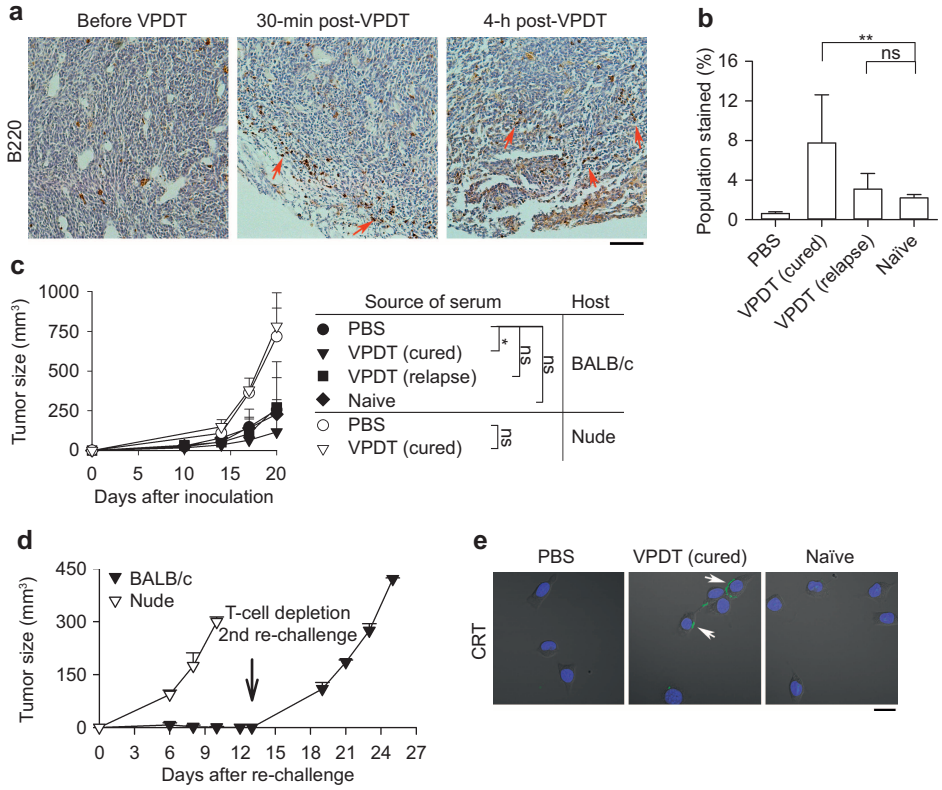

Figure 6 Involvement of humoral immune components in the VPDT-mediated immune response. (**a**) B-cell infiltration. After VPDT, paraffin tumor sections were stained with an anti-B220 antibody (brown). Arrows indicate the sites of B-cell infiltration. Bar = 200 μm. (**b**) Up-regulation of CT26-specific antibodies. CT26 tumor cells were incubated either with sera obtained from different groups of mice or with PBS, together with propidium iodide, followed by a secondary antibody against mouse IgG. Intact cells (propidium iodide^{-ve}) were analyzed by flow cytometry. Sera from naïve control, VPDT (cured) and VPDT (relapse) groups, $n = 6$, 10, and 6, respectively; PBS, $n = 3$. $^{**}p < 0.005$; ns, not significant. (**c**) Anti-tumor effects of serum. Filtered sera from different groups of mice or PBS were mixed with 2×10^5 CT26 cells. The suspension was inoculated subcutaneously into BALB/c mice or nude mice. Tumor growth was observed for 20 days. For the BALB/c mice, PBS control, $n = 11$; sera from the naïve control, VPDT (cured) and VPDT (relapse) groups, $n = 5$, 14, and 6, respectively. For the nude mice, PBS control, $n = 5$; serum from the VPDT (cured) group, $n = 5$. $^{*}p < 0.05$; ns, not significant. (**d**) Immunomodulatory effects of serum. On Day 20 after the first inoculation, a CT26 tumor cell re-challenge was given to the BALB/c and nude mice that had received the serum of the VPDT-cured mice. BALB/c mice, $n = 11$; nude mice, $n = 4$. The tumor size was monitored for 12 days. On Day 13 after re-challenge (indicated by the arrow), the BALB/c mice that had resisted tumor growth were depleted of T cells ($n = 3$). Then, they were given another round of tumor cell re-challenge, and the growth of the "third tumor" was monitored for 12 days. The data are shown as the means with S.D. (**e**) Serum-mediated cell surface CRT expression *in vitro*. CT26 tumor cells were treated with 10% serum of naïve mice or VPDT-cured mice in complete medium for 4 h at 37 °C. These cells were stained with an anti-CRT antibody (green) and Hoechst 33342 (blue). Arrows indicate the positions of CRT. Bar = 20 μm.

VPDT despite the PS itself (e.g., BAM-SiPc) showing little tumor specificity.

The immunogenicity of tumor cells could be strongly enhanced by the successful induction of DAMP expression during cytotoxic treatment. Among the various DAMPs, surface CRT plays a pivotal role in governing the activation of DCs and, hence, the adaptive immune response.[1,7] Although the pathway is different, PDT, like chemotherapy, could also lead to the expression of CRT on the cell surface.[47–49] For example, PDT with Photofrin, Hypericin, and Rose Bengal acetate has been shown to trigger the expression of CRT on the tumor cell surface *in vitro*.[8,50,51] The present study demonstrated that BAM-SiPc-PDT could induce the expression of surface CRT on CT26 tumor cells, together with two other DAMPs, HSP70, and HSP90, *in vitro* (Figure 1b and c). These surface-exposed HSPs have been reported to augment anti-tumor immunity by assisting DCs in acquiring and presenting tumor-derived antigens.[52,53]

The induction of surface CRT on tumor cells by PDT in an established tumor *in vivo* has hitherto been demonstrated only with Photofrin under classical conditions.[8] Whether VPDT could perform similarly is unknown. In our study, BAM-SiPc-VPDT induced a general up-regulation of CRT levels throughout the entire tumor (Figure 2c). More importantly, this CRT signal was detected on the tumor cell surface (Figure 2d). Because CRT can bind to damaged cells and CRT-associated tumor cells are more susceptible to cytotoxic lymphocyte attack,[7,19,54,55] the up-regulation of surface CRT in the treated tumor cells may, to a certain extent, contribute to the immunomodulatory effects of VPDT. The current VPDT treatment could induce the infiltration of DCs into the tumor region (Figure 2c). This observation is consistent with the

results of immunostimulatory chemotherapy using anthracyclines and with the presumed role of surface CRT as an "eat-me" signal on the stressed cells.[56,57]

VPDT-mediated anti-tumor immunity relies heavily on the activity of T cells.[58] The involvement of T cells in BAM-SiPc-VPDT-induced anti-tumor immunity was verified in the present study by (i) the presence of tumor-infiltrating $CD4^+$ and $CD8^+$ T cells (Figure 5a); (ii) the presence of cytotoxic lymphocytes against CT26 cells (Figure 5b); (iii) the secretion of T-cell-activating Th1 cytokines (IFN-γ and TNF-α) by splenocytes obtained from the VPDT-cured mice when co-cultured with CT26 cells (Figure 4); and (iv) the loss of anti-tumor immunity in the VPDT-cured mice after the depletion of T cells (Figure 5c).

Intriguingly, in addition to Th1 cytokines, Th2 cytokines (IL-4 and IL-10) that stimulate the humoral immune response were also detected in the same CT26 cell co-culture reaction (Figure 4). To the best of our knowledge, the simultaneous elevation of Th1 and Th2 cytokines has not been described in previous VPDT studies. Although similar observations have been reported in a few cancer vaccine studies, the implications remain unclear: some studies revealed a better therapeutic outcome, whereas others did not show any correlation.[59–61] Nevertheless, the increased secretion of Th2 cytokines by splenocytes indicates the potential involvement of B cells in the development of anti-tumor immunity.

The humoral immune response mediated by B cells is generally thought to be dispensable for anti-tumor immunity. In chemotherapy, the activity of B cells has been reported to strengthen resistance to the treatment of tumors in nude mice with anthracycline or oxaliplatin.[62,63] Nevertheless, there is accumulating evidence suggesting that tumor-infiltrating B cells are anti-tumor in nature because they can (i) exert direct cytotoxicity on tumor cells via TRAIL signaling, (ii) assist cell-mediated immunity with Th1 cytokine secretion, (iii) assist presentation of antigens to T cells via membrane-bound Ig molecules, and (iv) produce tumor-reactive antibodies.[64–66]

Tumor-reactive antibodies could, indeed, trigger anti-tumor immunity *in vivo*. In a human HER2 transgenic mouse model, anti-HER2 monoclonal antibody treatment of murine D5 melanoma transfected with full-length human HER2 led to tumor regression and the development of immunological memory against the original tumor.[67,68] The effects of antibodies can be affected by the antibodies' subclass, glycosylation state, and affinity toward various tumor-derived antigens;[69–71] therefore, it remains unknown whether tumor-reactive antibodies generated *in vivo* possess similar functions to those used in monoclonal antibody therapy.

In BALB/c mice, BAM-SiPc-VPDT successfully induced (i) the infiltration of B cells into CT26 tumors and (ii) elevated amounts of tumor-specific antibodies in the mice's serum (Figure 6a and b). These observations agree with those reported for WST11-VPDT but differ from the results of immunogenic chemotherapy using anthracycline, in which no tumor-specific antibodies could be boosted.[13,62] The serum of VPDT-cured mice, with no detectable IFN-γ or TNF-α (analyzed by ELISA, $n = 10$, data not shown), possessed anti-tumor properties that were T-cell-dependent (Figure 6c). These results are generally consistent with those reported in other studies. For example, Park *et al.* demonstrated that a monoclonal anti-HER2/neu antibody possessed a suppressive effect against TUBO (neu^+) tumors, but this anti-tumor effect disappeared in mice lacking functional lymphocytes.[72] Preise *et al.*[13] also reported that serum obtained from VPDT-cured mice could protect naïve mice from lung tumor metastasis, with the protective effect of the serum being dependent on the presence of functional lymphocytes in the host.

To determine whether the protective effect of the serum was due to the induction of anti-tumor immunity or simply the cytotoxic effects of serum factors, mice receiving the serum of VPDT-cured mice were given a tumor re-challenge. The tumor resistance observed in these mice suggested the involvement of an immune-related mechanism in the serum-mediated protection. The successful abolishment of this immunity by the removal of T cells using an anti-CD3 antibody or using nude mice confirmed the T-cell dependency of the serum-induced immune response (Figure 6d). Furthermore, the serum alone was not able to stimulate any immune response. In our preliminary study, BALB/c mice were injected with the serum of VPDT-cured mice with no co-administration of tumor cells. They were challenged with CT26 cells 20 days later. The tumors developed normally as in the control mice (data not shown). This observation suggested that certain interactions between the serum and the tumor cells are important for the induction of an immune response. Our results showed that the serum of VPDT-cured mice, but not naïve mice, could induce the expression of surface CRT in tumor cells *in vitro* (Figure 6e). Hence, it is possible that the serum functioned by stimulating the expression of surface CRT on tumor cells, which rendered the cells susceptible to attack by cytotoxic lymphocytes or favored their uptake by DCs.[7,54,55] The exact mechanism by which the serum mediates its tumor-suppressive effect and anti-tumor immune response is currently under investigation. One possibility is the involvement of Fc receptor-positive cells, which would account for the therapeutic effects of monoclonal antibodies.[72]

To summarize, the present study demonstrated that BAM-SiPc-VPDT could activate anti-tumor immunity in a T-cell-dependent manner. In addition, the humoral immune response was involved in terms of the elevation of tumor-specific antibodies in the mouse serum after treatment. The serum of VPDT-cured mice could mimic the effect of monoclonal antibody therapy *in vivo* by protecting the mice against tumor re-challenge, suggesting the involvement of B cells in the mechanism of VPDT-induced anti-tumor immunity. A combination of VPDT with an immunomodulatory agent that strengthens antibody production may be a novel therapeutic approach against cancer in the future.

COMPETING INTERESTS

The authors declare no conflicts of interest.

1 Tesniere A, Schlemmer F, Boige V, Kepp O, Martins I, Ghiringhelli F *et al*. Immunogenic death of colon cancer cells treated with oxaliplatin. *Oncogene* 2010; **29**: 482–491.
2 Gorin J-B, Ménager J, Gouard S, Maurel C, Guilloux Y, Faivre-Chauvet A *et al*. Antitumor immunity induced after α irradiation. *Neoplasia* 2014; **16**: 319–328.
3 Veenstra JJ, Gibson HM, Littrup PJ, Reyes JD, Cher ML. Cryotherapy with concurrent CpG oligonucleotide treatment controls local tumor recurrence and modulates HER2/neu immunity. *Cancer Res* 2014; **74**: 5409–5420.
4 Krysko DV, Garg AD, Kaczmarek A, Krysko O, Agostinis P, Vandenabeele P. Immunogenic cell death and DAMPs in cancer therapy. *Nat Rev Cancer* 2012; **12**: 860–875.
5 Obeid M, Panaretakis T, Tesniere A, Joza N, Tufi R, Apetoh L *et al*. Leveraging the immune system during chemotherapy: moving calreticulin to the cell surface converts apoptotic death from "silent" to immunogenic. *Cancer Res* 2007; **67**: 7941–7944.
6 Agostinis P, Berg K, Cengel KA, Foster TH, Girotti AW, Gollnick SO *et al*. Photodynamic therapy of cancer: an update. *CA Cancer J Clin* 2011; **61**: 250–281.
7 Obeid M, Tesniere A, Ghiringhelli F, Fimia GM, Apetoh L, Perfettini J-L *et al*. Calreticulin exposure dictates the immunogenicity of cancer cell death. *Nat Med* 2007; **13**: 54–61.
8 Korbelik M, Zhang W, Merchant S. Involvement of damage-associated molecular patterns in tumor response to photodynamic therapy: surface expression of calreticulin and high-mobility group box-1 release. *Cancer Immunol Immunother* 2011; **60**: 1431–1437.
9 Adkins I, Fucikova J, Garg AD, Agostinis P, Špíšek R. Physical modalities inducing immunogenic tumor cell death for cancer immunotherapy. *Oncoimmunology* 2015; **3**: e968434.
10 Chiaviello A, Postiglione I, Palumbo G. Targets and mechanisms of photodynamic therapy in lung cancer cells: a brief overview. *Cancers (Basel)* 2011; **3**: 1014–1041.
11 Garg AD, Nowis D, Golab J, Agostinis P. Photodynamic therapy: illuminating the road from cell death towards anti-tumour immunity. *Apoptosis* 2010; **15**: 1050–1071.
12 Starkey JR, Pascucci EM, Drobizhev MA, Elliott A, Rebane AK. Vascular targeting to the SST2 receptor improves the therapeutic response to near-IR two-photon activated PDT for deep-tissue cancer treatment. *Biochim Biophys Acta* 2013; **1830**: 4594–4603.
13 Preise D, Oren R, Glinert I, Kalchenko V, Jung S, Scherz A *et al*. Systemic antitumor protection by vascular-targeted photodynamic therapy involves cellular and humoral immunity. *Cancer Immunol Immunother* 2009; **58**: 71–84.
14 Dolmans DE, Kadambi A, Hill JS, Waters CA, Robinson BC, Walker JP *et al*. Vascular accumulation of a novel photosensitizer, MV6401, causes selective thrombosis in tumor vessels after photodynamic therapy. *Cancer Res* 2002; **62**: 2151–2156.
15 Fong WP, Yeung HY, Lo PC, Ng DK. Photodynamic therapy. In: Ho AH, Kim D, Somekh MG (eds.) *Handbook of photonics for biomedical engineering*. Dordrecht: Springer Science+Business Media, 2014: 1–20.
16 Castano AP, Mroz P, Hamblin MR. Photodynamic therapy and anti-tumour immunity. *Nat Rev Cancer* 2006; **6**: 535–545.
17 Castano AP, Demidova TN, Hamblin MR. Mechanisms in photodynamic therapy: part three-photosensitizer pharmacokinetics, biodistribution, tumor localization and modes of tumor destruction. *Photodiagnosis Photodyn Ther* 2005; **2**: 91–106.
18 Korbelik M, Krosl G. Photofrin accumulation in malignant and host cell populations of various tumours. *Br J Cancer* 1996; **73**: 506–513.
19 Korbelik M, Hamblin MR. The impact of macrophage-cancer cell interaction on the efficacy of photodynamic therapy. *Photochem Photobiol Sci* 2015; **14**: 1403–1409.
20 Hamblin MR, Newman EL. On the mechanism of the tumour-localising effect in photodynamic therapy. *J Photochem Photobiol B* 1994; **23**: 3–8.
21 Byrne AT, O'Connor AE, Hall M, Murtagh J, O'Neill K, Curran KM *et al*. Vascular-targeted photodynamic therapy with BF2-chelated Tetraaryl-Azadipyrromethene agents: a multi-modality molecular imaging approach to therapeutic assessment. *Br J Cancer* 2009; **101**: 1565–1573.
22 Firczuk M, Nowis D, Golab J. PDT-induced inflammatory and host responses. *Photochem Photobiol Sci* 2011; **10**: 653–663.
23 Brackett CM, Gollnick SO. Photodynamic therapy enhancement of anti-tumor immunity. *Photochem Photobiol Sci* 2011; **10**: 649–652.
24 Reginato E, Wolf P, Hamblin MR. Immune response after photodynamic therapy increases anti-cancer and anti-bacterial effects. *World J Immunol* 2012; **29**: 997–1003.
25 Korbelik M, Krosl G, Krosl J, Dougherty GJ. The role of host lymphoid populations in the response of mouse EMT6 tumor to photodynamic therapy. *Cancer Res* 1996; **56**: 5647–5652.
26 Fingar VH, Kik PK, Haydon PS, Cerrito PB, Tseng M, Abang E *et al*. Analysis of acute vascular damage after photodynamic therapy using benzoporphyrin derivative (BPD). *Br J Cancer* 1999; **79**: 1702–1708.
27 Chen B, Pogue BW, Goodwin IA, O'Hara JA, Wilmot CM, Hutchins JE *et al*. Blood flow dynamics after photodynamic therapy with verteporfin in the RIF-1 tumor. *Radiat Res* 2003; **160**: 452–459.
28 Woodhams JH, MacRobert AJ, Novelli M, Bown SG. Photodynamic therapy with WST09 (Tookad): quantitative studies in normal colon and transplanted tumours. *Int J Cancer* 2006; **118**: 477–482.
29 Chen B, Pogue BW, Zhou X, O'Hara JA, Solban N, Demidenko E *et al*. Effect of tumor host microenvironment on photodynamic therapy in a rat prostate tumor model. *Clin Cancer Res* 2005; **11**: 720–727.
30 Sanovic R, Verwanger T, Hartl A, Krammer B. Low dose hypericin-PDT induces complete tumor regression in BALB/c mice bearing CT26 colon carcinoma. *Photodiagnosis Photodyn Ther* 2011; **8**: 291–296.
31 Castano AP, Mroz P, Wu MX, Hamblin MR. Photodynamic therapy plus low-dose cyclophosphamide generates antitumor immunity in a mouse model. *Proc Natl Acad Sci USA* 2008; **105**: 5495–5500.
32 Chen B, Roskams T, de Witte PA. Antivascular tumor eradication by hypericin-mediated photodynamic therapy. *Photochem Photobiol* 2002; **76**: 509–513.
33 Delaey E, Zupko I, Chen B, Derycke A, van Laar F, De Vos D *et al*. Comparison of hexamethylhypericin and tetrabromohypericin to hypericin for their *in vivo* efficacy as PDT tools. *Int J Oncol* 2003; **23**: 519–524.
34 Lassalle HP, Dumas D, Gräfe S, D'Hallewin MA, Guillemin F, Bezdetnaya L. Correlation between *in vivo* pharmacokinetics, intratumoral distribution and photodynamic efficiency of liposomal mTHPC. *J Control Release* 2009; **134**: 118–124.
35 Li LB, Luo RC. Effect of drug-light interval on the mode of action of Photofrin photodynamic therapy in a mouse tumor model. *Lasers Med Sci* 2009; **24**: 597–603.
36 Lo PC, Huang JD, Cheng DYY, Chan EYM, Fong WP, Ko WH *et al*. New amphiphilic silicon(IV) phthalocyanines as efficient photosensitizers for photodynamic therapy: synthesis, photophysical properties, and *in vitro* photodynamic activities. *Chemistry* 2004; **10**: 4831–4838.
37 Lo PC, Leung SC, Chan EY, Fong WP, Ko WH, Ng DK. Photodynamic effects of a novel series of silicon(IV) phthalocyanines against human colon adenocarcinoma cells. *Photodiagnosis Photodyn Ther* 2007; **4**: 117–123.
38 Lai JC, Lo PC, Ng DK, Ko WH, Leung SC, Fung KP *et al*. BAM-SiPc, a novel agent for photodynamic therapy, induces apoptosis in human hepatocarcinoma HepG2 cells by a direct mitochondrial action. *Cancer Biol Ther* 2006; **5**: 413–418.
39 Leung SC, Lo PC, Ng DK, Liu WK, Fung KP, Fong WP. Photodynamic activity of BAM-SiPc, an unsymmetrical bisamino silicon(IV) phthalocyanine, in tumour-bearing nude mice. *Br J Pharmacol* 2008; **154**: 4–12.
40 Obeid M, Panaretakis T, Joza N, Tufi R, Tesniere A, van Endert P *et al*. Calreticulin exposure is required for the immunogenicity of gamma-irradiation and UVC light-induced apoptosis. *Cell Death Differ* 2007; **14**: 1848–1850.
41 Reginato E, Mroz P, Chung H, Kawakubo M, Wolf P, Hamblin MR. Photodynamic therapy plus regulatory T-cell depletion produces immunity against a mouse tumour that expresses a self-antigen. *Br J Cancer* 2013; **109**: 2167–2174.

42 Castano AP, Liu Q, Hamblin MR. A green fluorescent protein-expressing murine tumour but not its wild-type counterpart is cured by photodynamic therapy. *Br J Cancer* 2006; **94**: 391–397.
43 Mroz P, Vatansever F, Muchowicz A, Hamblin MR. Photodynamic therapy of murine mastocytoma induces specific immune responses against the cancer/testis antigen P1A. *Cancer Res* 2013; **73**: 6462–6470.
44 Mroz P, Szokalska A, Wu MX, Hamblin MR. Photodynamic therapy of tumors can lead to development of systemic antigen-specific immune response. *PLoS One* 2010; **5**: e15194.
45 García-Díaz M, Kawakubo M, Mroz P, Sagristà ML, Mora M, Nonell S *et al*. Cellular and vascular effects of the photodynamic agent temocene are modulated by the delivery vehicle. *J Control Release* 2012; **162**: 355–363.
46 Bhuvaneswari R, Gan YY, Lucky SS, Chin WW, Ali SM, Soo KC *et al*. Molecular profiling of angiogenesis in hypericin mediated photodynamic therapy. *Mol Cancer* 2008; **7**: 56.
47 Panaretakis T, Joza N, Modjtahedi N, Tesniere A, Vitale I, Durchschlag M *et al*. The co-translocation of ERp57 and calreticulin determines the immunogenicity of cell death. *Cell Death Differ* 2008; **15**: 1499–1509.
48 Panaretakis T, Kepp O, Brockmeier U, Tesniere A, Bjorklund A-C, Chapman DC *et al*. Mechanisms of pre-apoptotic calreticulin exposure in immunogenic cell death. *EMBO J* 2009; **28**: 578–590.
49 Garg AD, Krysko DV, Verfaillie T, Kaczmarek A, Ferreira GB, Marysael T *et al*. A novel pathway combining calreticulin exposure and ATP secretion in immunogenic cancer cell death. *EMBO J* 2012; **31**: 1062–1079.
50 Garg AD, Krysko DV, Vandenabeele P, Agostinis P. Hypericin-based photodynamic therapy induces surface exposure of damage-associated molecular patterns like HSP70 and calreticulin. *Cancer Immunol Immunother* 2012; **61**: 215–221.
51 Panzarini E, Inguscio V, Fimia GM, Dini L. Rose Bengal acetate photodynamic therapy (RBAc-PDT) induces exposure and release of damage-associated molecular patterns (DAMPs) in human HeLa cells. *PLoS One* 2014; **9**: e105778.
52 Green DR, Ferguson T, Zitvogel L, Kroemer G. Immunogenic and tolerogenic cell death. *Nat Rev Immunol* 2009; **9**: 353–363.
53 Garg AD, Nowis D, Golab J, Vandenabeele P, Krysko DV, Agostinis P. Immunogenic cell death, DAMPs and anticancer therapeutics: an emerging amalgamation. *Biochim Biophys Acta* 2010; **1805**: 53–71.
54 Hodge JW, Garnett CT, Farsaci B, Palena C, Tsang KY, Ferrone S *et al*. Chemotherapy-induced immunogenic modulation of tumor cells enhances killing by cytotoxic T lymphocytes and is distinct from immunogenic cell death. *Int J Cancer* 2013; **133**: 624–636.
55 Gameiro SR, Jammeh ML, Wattenberg MM, Tsang KY, Ferrone S, Hodge JW. Radiation-induced immunogenic modulation of tumor enhances antigen processing and calreticulin exposure, resulting in enhanced T-cell killing. *Oncotarget* 2014; **5**: 403–416.
56 Ma Y, Adjemian S, Mattarollo SR, Yamazaki T, Aymeric L, Yang H *et al*. Anticancer chemotherapy-induced intratumoral recruitment and differentiation of antigen-presenting cells. *Immunity* 2013; **38**: 729–741.
57 Gardai SJ, McPhillips KA, Frasch SC, Janssen WJ, Starefeldt A, Murphy-Ullrich JE *et al*. Cell-surface calreticulin initiates clearance of viable or apoptotic cells through trans-activation of LRP on the phagocyte. *Cell* 2005; **123**: 321–334.
58 Anzengruber F, Avci P, de Freitas LF, Hamblin MR. T-cell mediated anti-tumor immunity after photodynamic therapy: why does it not always work and how can we improve it? *Photochem Photobiol Sci* 2015; **14**: 1492–1509.
59 Kyte JA, Trachsel S, Risberg B, Thor Straten P, Lislerud K, Gaudernack G. Unconventional cytokine profiles and development of T cell memory in long-term survivors after cancer vaccination. *Cancer Immunol Immunother* 2009; **58**: 1609–1626.
60 Mortara L, Balza E, Sassi F, Castellani P, Carnemolla B, De Lerma Barbaro A *et al*. Therapy-induced antitumor vaccination by targeting tumor necrosis factor-α to tumor vessels in combination with melphalan. *Eur J Immunol* 2007; **37**: 3381–3392.
61 Pohla H, Buchner A, Stadlbauer B, Frankenberger B, Stevanovic S, Walter S *et al*. High immune response rates and decreased frequencies of regulatory T cells in metastatic renal cell carcinoma patients after tumor cell vaccination. *Mol Med* 2012; **18**: 1499–1508.
62 Hannani D, Locher C, Yamazaki T, Colin-Minard V, Vetizou M, Aymeric L *et al*. Contribution of humoral immune responses to the antitumor effects mediated by anthracyclines. *Cell Death Differ* 2014; **21**: 50–58.
63 Shalapour S, Font-Burgada J, Di Caro G, Zhong Z, Sanchez-Lopez E, Dhar D *et al*. Immunosuppressive plasma cells impede T-cell-dependent immunogenic chemotherapy. *Nature* 2015; **521**: 94–98.
64 Nelson BH. $CD20^+$ B cells: the other tumor-infiltrating lymphocytes. *J Immunol* 2010; **185**: 4977–4982.
65 Linnebacher M, Maletzki C. Tumor-infiltrating B cells: the ignored players in tumor immunology. *Oncoimmunology* 2012; **1**: 1186–1188.
66 Shen P, Fillatreau S. Antibody-independent functions of B cells: a focus on cytokines. *Nat Rev Immunol* 2015; **15**: 441–451.
67 Wang S, Astsaturov IA, Bingham CA, McCarthy KM, Von Mehren M, Xu W *et al*. Effective antibody therapy induces host-protective antitumor immunity that is augmented by TLR4 agonist treatment. *Cancer Immunol Immunother* 2012; **61**: 49–61.
68 Surana R, Wang S, Xu W, Jablonski SA, Weiner LM. IL4 limits the efficacy of tumor-targeted antibody therapy in a murine model. *Cancer Immunol Res* 2014; **2**: 1103–1112.
69 Ann W, Morrison S. Effect of glycosylation on antibody function: implications for genetic engineering. *Trends Biotechnol* 1997; **15**: 26–32.
70 Patel D, Guo X, Ng S, Melchior M, Balderes P, Burtrum D *et al*. IgG isotype, glycosylation, and EGFR expression determine the induction of antibody-dependent cellular cytotoxicity *in vitro* by cetuximab. *Hum Antibodies* 2010; **19**: 89–99.
71 Kubach J, Hubo M, Amendt C, Stroh C, Jonuleit H. IgG1 anti-epidermal growth factor receptor antibodies induce CD8-dependent antitumor activity. *Int J Cancer* 2014; **136**: 821–830.
72 Park S, Jiang Z, Mortenson ED, Deng L, Radkevich-Brown O, Yang X *et al*. The therapeutic effect of anti-HER2/neu antibody depends on both innate and adaptive immunity. *Cancer Cell* 2010; **18**: 160–170.